ISSN No:-2456-2165 https://doi.org/10.38124/ijisrt/26jul1844

Heavy Metal Removal from Aqueous Media Using Lignocellulosic Waste Material (Corn Stalk)

Ndukwu D. E.[1*]; Ogukwe C. E.[2]; Enenebeaku C. K.[3]; Akalezi C. O.[4]; Didacus D. E.[5]; Chukwueke K. A.[6]; Igbomezie M. C.[7]

[1]Department of Chemistry, Federal College of Education (Technical), Omoku, Rivers State, Nigeria
[2,3,4,6,7]Department of Chemistry, Federal University of Technology, Owerri (FUTO), Nigeria
[5]Department of Petroleum and Gas Engineering, Nigeria Maritime University, Delta State, Nigeria

Corresponding Author: Ndukwu, D. E.[1*]

Publication Date: 2026/08/17

Abstract: Corn stalk (*Zea mays*, designated COS) is generated in massive quantities following maize grain harvest and remains underutilized in most agricultural systems, particularly across sub-Saharan Africa. This study investigated the potential of COS as a low-cost biosorbent for the removal of Pb(II), Zn(II), Cu(II), Cr(VI), and Ni(II) ions from aqueous solution through systematic batch adsorption experiments. The effects of contact time (30–180 min), adsorbent dose (1–5 g), initial metal concentration (10–90 mg/L), solution pH (2–10), and temperature (30–70°C) were each evaluated. Among the five metals studied, nickel achieved the highest removal, reaching 97.0% at 180 minutes, while lead demonstrated exceptional concentration independence, maintaining 90% removal efficiency across the entire 10–50 mg/L range. Chromium showed peak adsorption at pH 2 (67%), consistent with electrostatic attraction of chromate anions to protonated surface sites, while the four cationic metals performed best at pH 6. Unlike many lignocellulosic biosorbents, equilibrium data for all five metals including Cr(VI) conformed to the Langmuir isotherm model (R^2 = 0.957–0.998), indicating predominantly monolayer adsorption on a comparatively homogeneous set of binding sites across the tubular, lignocellulosic COS matrix. The Pseudo-Second-Order kinetic model provided an excellent fit for all metals (R^2 = 0.997–0.999), with calculated equilibrium capacities closely matching experimental values, implicating chemisorption as the dominant rate-controlling mechanism. Thermodynamic analysis yielded negative ΔG° (−0.414 to −0.731 kJ/mol), negative ΔH°, and positive ΔS° values for all five metals, confirming that adsorption is spontaneous, mildly exothermic, and entropically driven. Scanning electron micrographs showed the characteristic rough tubular pre-adsorption texture becoming densely aggregated after metal loading, while FTIR spectroscopy identified hydroxyl, carboxylic, thiol, and aliphatic C–H groups as primary binding sites, with post-adsorption shifts in the O–H stretching region confirming metal–ligand complexation. These findings establish COS as a high-performing, and readily available biosorbent for metal water remediation.

Keywords: *Biosorption; Corn Stalk; Zea Mays; Heavy Metals; Langmuir Isotherm; Pseudo-Second-Order Kinetics; Thermodynamics; Agricultural Waste; Wastewater Treatment.*

How to Cite: Ndukwu D. E.; Ogukwe C. E.; Enenebeaku C. K.; Akalezi C. O.; Didacus D. E.; Chukwueke K. A.; Igbomezie M. C. (2026) Heavy Metal Removal from Aqueous Media Using Lignocellulosic Waste Material (Corn Stalk). *International Journal of Innovative Science and Research Technology*, 11(7), 3743-3757. https://doi.org/10.38124/ijisrt/26jul1844

I. INTRODUCTION

The release of heavy metal-laden effluents into freshwater systems continues to represent one of the most persistent and widespread environmental challenges of the present era, with electroplating, tannery, battery manufacturing, pigment production, and metal-refining industries collectively contributing lead, zinc, copper, chromium, and nickel to surface and groundwater bodies at rates that frequently exceed safe ambient thresholds (Mitra et al., 2022). These metallic contaminants are non-biodegradable, accumulate progressively through the food chain, and exert toxicological effects on aquatic organisms and human populations even at trace concentrations (Bilal et al., 2022).

The clinical profile of these metals is well-established and it calls for concern. Lead causes irreversible neurological damage in children and promotes cardiovascular disease and renal failure in adults. Hexavalent chromium, the more soluble and mobile valence state, is a confirmed human carcinogen with mutagenic properties and a strong capacity for cellular oxidative stress (Balali-Mood et al., 2021). Nickel exposure at elevated levels contributes to contact hypersensitivity and bronchial carcinoma, while zinc and copper, despite their biological roles as trace micronutrients,

ISSN No:-2456-2165 https://doi.org/10.38124/ijisrt/26jul1844

become systemically toxic at concentrations encountered in industrial discharges (Genchi et al., 2023). Regulatory agencies globally, guided by WHO drinking-water quality guidelines, impose strict maximum permissible concentrations for each of these elements, compelling industries to invest in effective water treatment solutions (WHO, 2022).

Conventional treatment technologies — including lime precipitation, ion exchange, coagulation-flocculation, membrane separation, and electrocoagulation — achieve acceptable heavy metal removal but impose prohibitive costs, particularly when operating at small scale or in resource-limited settings (Vunain et al., 2023). The generation of metal-concentrated sludge requiring safe disposal adds a further environmental and economic burden. Adsorption using agricultural residue-derived biosorbents offers a compelling alternative to many of these disadvantages: the feedstocks are essentially free, require minimal processing, and are available locally in large quantities across agricultural regions (Raji et al., 2023).

Corn (*Zea mays*) is one of the world's most extensively cultivated cereal crops. Global maize production generates hundreds of millions of tonnes of stalk residue annually, much of which is burned in fields or left to decompose with minimal benefit. Corn stalk has a distinctly tubular, vascular lignocellulosic structure whose cell walls contain cellulose, hemicellulose, and lignin in proportions that yield a measurable density of hydroxyl, carboxyl, and other oxygen-bearing functional groups capable of coordinating metal cations and anions through surface complexation and electrostatic attraction (Liang et al., 2023). A small but growing body of literature has demonstrated meaningful metal uptake onto corn stalk and related maize residues, though comprehensive multi-metal assessments across the full parameter space — including simultaneous kinetic, isotherm, thermodynamic, and spectroscopic evaluation — remain comparatively scarce (Mthombeni et al., 2023).

This study presents a systematic investigation of corn stalk biosorbent (COS) for the removal of Pb(II), Zn(II), Cu(II), Cr(VI), and Ni(II) from aqueous solution. Batch experiments were designed to quantify the influence of contact time, adsorbent dose, initial metal concentration, solution pH, and temperature on removal efficiency and adsorption capacity. The equilibrium data were modeled using Langmuir and Freundlich isotherms, kinetics were analyzed with Pseudo-First-Order and Pseudo-Second-Order models, and thermodynamic parameters were derived from temperature-dependent equilibria. Surface characterization was performed before and after metal loading using scanning electron microscopy and FTIR spectroscopy. The study provides a comprehensive basis for COS application in low-cost multi-metal wastewater treatment.

II. MATERIALS AND METHODS

➢ *Biosorbent Collection and Preparation*

Corn stalk residue (*Zea mays*) was harvested from farmland in Omoku, Rivers State, Nigeria, following grain collection. The stalks were cut into smaller segments and washed several times under running tap water to dislodge adhering soil, dust, and plant debris, followed by thorough rinsing with deionized water. After preliminary shade-drying, the material was oven-dried at 60°C until constant weight was achieved. The dried stalks were pulverized in a laboratory mill and sieved to a uniform particle size of 300 µm. The resulting COS powder was stored in sealed polyethylene bags at ambient temperature until use.

➢ *Preparation of Metal Ion Solutions*

Analytical-grade lead(II) chloride ($PbCl_2$), copper(II) tetraoxosulphate(VI) pentahydrate ($CuSO_4 \cdot 5H_2O$), zinc(II) chloride ($ZnCl_2$), nickel(II) chloride hexahydrate ($NiCl_2 \cdot 6H_2O$), and potassium dichromate ($K_2Cr_2O_7$) were each dissolved in deionized water to prepare 1000 mg/L stock solutions in 1-litre volumetric flasks. Working solutions at concentrations of 10, 30, 50, 70, and 90 mg/L were obtained by serial dilution.

➢ *Batch Adsorption Procedure*

Each batch experiment involved contacting 1 g of COS with 100 mL of the appropriate metal ion solution in 250-mL conical flasks, shaken at 200 rpm on an orbital shaker. At predetermined time points, aliquots were withdrawn, filtered through Whatman 0.45 µm membrane filters, and the filtrate analyzed for residual metal concentration by Atomic Absorption Spectrophotometry. Percentage removal (R%) and equilibrium adsorption capacity (qe, mg/g) were calculated as:

$$R\% = [(C_0 - Ce) / C_0] \times 100$$

$$qe = [(C_0 - Ce) \times V] / m$$

Where C_0 and Ce are the initial and equilibrium metal concentrations (mg/L), V is the solution volume (L), and m is the adsorbent mass (g). The operational variables studied were contact time (30–180 min), adsorbent dose (1–5 g), initial metal concentration (10–90 mg/L), solution pH (2–10, adjusted with 0.1 M HCl or 0.1 M NaOH), and temperature (30–70°C controlled via a thermostated water bath).

➢ *Equilibrium Isotherm Models*

Equilibrium data were fitted to linearized Langmuir and Freundlich isotherm models. The Langmuir model assumes monolayer adsorption on a homogeneous surface:

$$Ce/qe = 1/(qm \cdot KL) + Ce/qm$$

Where qm (mg/g) is the maximum monolayer adsorption capacity and KL (L/mg) is the Langmuir equilibrium constant. The Freundlich model, which describes adsorption on heterogeneous surfaces, is given by:

$$\log qe = \log KF + (1/n) \log Ce$$

Where KF is the Freundlich capacity constant and 1/n is the heterogeneity index; values of 1/n below unity indicate favorable adsorption (Foo & Hameed, 2010).

ISSN No:-2456-2165 https://doi.org/10.38124/ijisrt/26jul1844

➢ *Kinetic Models*

Time-dependent uptake data were analyzed with the Pseudo-First-Order (PFO) model of Lagergren (1898) and the Pseudo-Second-Order (PSO) model of Ho and McKay (1999):

$$PFO: \log(qe - qt) = \log qe - (k_1/2.303)t$$

$$PSO: t/qt = 1/(k_2 qe^2) + t/qe$$

Model selection was based on the coefficient of determination (R^2) and the agreement between calculated (qe,cal) and experimental (qe,exp) equilibrium capacities.

➢ *Thermodynamic Analysis*

Thermodynamic parameters were derived from the temperature-dependent equilibrium distribution coefficient Kc (= qe/Ce) using the van't Hoff equation:

$$\ln Kc = \Delta S°/R - \Delta H°/RT; \quad \Delta G° = -RT \ln Kc$$

Where R = 8.314 J/mol·K and T is the absolute temperature. ΔH° and ΔS° were obtained from the slope and intercept of the ln Kc vs. 1/T plot (Adeyemo et al., 2022).

➢ *Surface Characterization*

The surface morphology of COS before and after adsorption was examined using Scanning Electron Microscopy (SEM) at 2000× magnification. Fourier Transform Infrared (FTIR) spectroscopy was used to identify surface functional groups and track spectral changes resulting from metal binding, scanning across 400–4000 cm^{-1}.

III. RESULTS AND DISCUSSION

➢ *Optimal Batch Adsorption Conditions*

Preliminary batch experiments identified the optimal operating conditions for each metal–COS system, as summarized in Table 1.

Table 1 Optimal Batch Adsorption Conditions for Heavy Metal Removal by COS

Metal Ion	Optimum Time (min)	Dose (g)	Init. Conc. (mg/L)	pH	Temp (°C)
Pb^{2+}	90	3	50	6	40
Zn^{2+}	30	3	30	6	30
Cu^{2+}	60	3	50	6	40
Cr	90	2	40	2	30
Ni^{2+}	30	2	50	4	30

Several important distinctions are apparent from Table 1. First, the optimal pH for cationic metals — Pb^{2+}, Zn^{2+}, Cu^{2+} — was pH 6, while Cr required strongly acidic conditions at pH 2. This contrast is significant: at pH 2, protonation of hydroxyl and carboxyl groups on the COS surface generates a net positive charge, creating strong electrostatic attraction for the anionic chromate species ($HCrO_4^-$ and $Cr_2O_7^{2-}$) that dominate Cr(VI) speciation under those conditions (Akhtar et al., 2024). Nickel stands apart from the other cationic metals in requiring a slightly more acidic optimum of pH 4, which may reflect competitive deprotonation dynamics at the lignocellulosic surface that are subtly different for Ni^{2+} compared to the other divalent cations. The longer equilibrium time required for Pb^{2+} and Cr (90 min) compared to Zn^{2+} and Ni^{2+} (30 min) indicates slower diffusion kinetics for these metals toward the binding sites within the COS matrix, consistent with the different molecular masses and hydration shell energies involved.

➢ *Effect of Contact Time*

The variation in metal uptake by COS over 30–180 minutes is reported in Table 2 and illustrated graphically in Figure 1.

Table 2 Effect of Contact Time on Heavy Metal Adsorption Onto COS

Metal	Time (min)	Vol (L)	C_0 (mg/L)	Ce (mg/L)	qe (mg/g)	% Removal
Pb^{2+}	30	0.108	50	20.0	1.11	60.0
	60	0.105	50	12.0	1.33	76.0
	90	0.107	50	4.5	1.42	91.0
	120	0.104	50	4.0	1.38	92.0
	150	0.106	50	3.5	1.46	93.0
	180	0.103	50	3.2	1.51	93.6
Zn^{2+}	30	0.103	30	12.0	0.62	60.0
	60	0.106	30	4.5	0.85	85.0
	90	0.101	30	4.0	0.86	86.7
	120	0.107	30	3.5	0.88	88.3
	150	0.105	30	3.0	0.90	90.0
	180	0.108	30	2.7	0.92	91.0
Cu^{2+}	30	0.108	50	18.0	1.05	64.0
	60	0.105	50	7.5	1.42	85.0
	90	0.107	50	6.5	1.45	87.0
	120	0.104	50	5.5	1.49	89.0

ISSN No:-2456-2165 https://doi.org/10.38124/ijisrt/26jul1844

	150	0.106	50	4.5	1.53	91.0
	180	0.102	50	4.0	1.57	92.0
Cr	30	0.102	40	6.0	1.70	85.0
	60	0.104	40	5.0	1.75	87.5
	90	0.108	40	4.0	1.78	90.0
	120	0.105	40	3.2	1.84	92.0
	150	0.107	40	2.6	1.87	93.5
	180	0.103	40	2.2	1.92	94.5
Ni^{2+}	30	0.107	50	4.5	2.28	91.0
	60	0.105	50	3.5	2.38	93.0
	90	0.108	50	2.8	2.47	94.4
	120	0.104	50	2.2	2.50	95.6
	150	0.106	50	1.8	2.57	96.4
	180	0.101	50	1.5	2.63	97.0

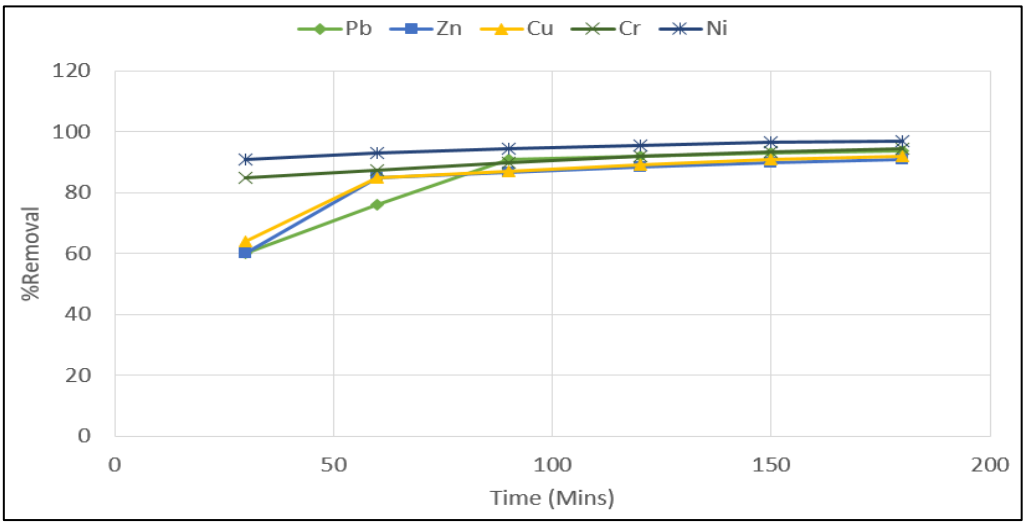

Fig 1 Effect of Contact Time on the Percentage Removal of Pb^{2+} , Zn^{2+}, Cu^{2+}, Cr, and Ni^{2+} onto COS.

All five metals exhibited the characteristic two-stage adsorption profile: a rapid initial uptake driven by the abundance of unoccupied surface sites, followed by a progressively slower approach to equilibrium as site availability diminishes and residual metal concentration in solution decreases (Bashir et al., 2023). Lead removal rose from 60% at 30 minutes to 91% at 90 minutes, plateauing near 93–93.6% by 150–180 minutes, confirming 90 minutes as the practical equilibrium time. Zinc showed similarly rapid early kinetics, climbing from 60% at 30 minutes to 85% at 60 minutes, and continuing a more gradual rise to 91% at 180 minutes, with the selected optimum at 30 minutes reflecting the point of meaningful early-stage uptake.

Copper removal increased from 64% at 30 minutes to 85% at 60 minutes, then climbed steadily to 92% at 180 minutes, reflecting a progressive occupation of multiple site types on the COS surface, including readily accessible surface hydroxyl groups and slower-diffusing intraparticle binding sites. Chromium demonstrated strong and rapid initial uptake from the 40 mg/L solution, achieving 85% removal within the first 30 minutes and rising to 94.5% by 180 minutes — among the highest removals recorded for chromate on an unmodified lignocellulosic adsorbent without chemical pre-treatment (Onyancha et al., 2024). Nickel produced the most exceptional performance of all five metals: starting at 91.0% at just 30 minutes and increasing to 97.0% at 180 minutes, indicating an exceptionally strong and rapid affinity between Ni^{2+} and the functional groups present on the COS surface at pH 4, which likely includes deprotonated carboxylate and hydroxyl sites ideally suited to coordinate nickel in its preferred octahedral coordination geometry.

➢ *Effect of Adsorbent Dose*

The influence of COS dose on metal removal efficiency and adsorption capacity was examined over 1–5 g per 100 mL. Results are presented in Table 3.

Table 3 Effect of Adsorbent Dose on Heavy Metal Adsorption Onto COS

Metal	**Dose (g)**	**Vol (L)**	**C_0 (mg/L)**	**Ce (mg/L)**	**qe (mg/g)**	**% Removal**
Pb^{2+}	1.0	0.108	50	20.0	3.24	60.0
	2.0	0.105	50	12.0	1.90	76.0
	3.0	0.107	50	4.5	1.42	91.0
	4.0	0.104	50	3.0	1.22	94.0

ISSN No:-2456-2165 https://doi.org/10.38124/ijisrt/26jul1844

	5.0	0.106	50	2.0	1.13	96.0
Zn^{2+}	1.0	0.103	30	15.0	1.55	50.0
	2.0	0.106	30	10.0	1.06	66.7
	3.0	0.101	30	4.5	0.85	85.0
	4.0	0.107	30	3.0	0.72	90.0
	5.0	0.105	30	2.0	0.59	93.3
Cu^{2+}	1.0	0.108	50	22.0	2.91	56.0
	2.0	0.105	50	15.0	1.67	70.0
	3.0	0.107	50	7.5	1.42	85.0
	4.0	0.104	50	5.0	1.17	90.0
	5.0	0.106	50	3.5	1.10	93.0
Cr	1.0	0.102	40	20.0	2.06	50.0
	2.0	0.104	40	6.0	1.70	85.0
	3.0	0.108	40	4.0	1.33	90.0
	4.0	0.105	40	2.5	0.98	93.8
	5.0	0.107	40	1.5	0.82	96.3
Ni^{2+}	1.0	0.107	50	20.0	3.18	60.0
	2.0	0.108	50	4.5	2.28	91.0
	3.0	0.104	50	3.0	1.51	94.0
	4.0	0.106	50	2.0	1.27	96.0
	5.0	0.105	50	1.5	1.16	97.0

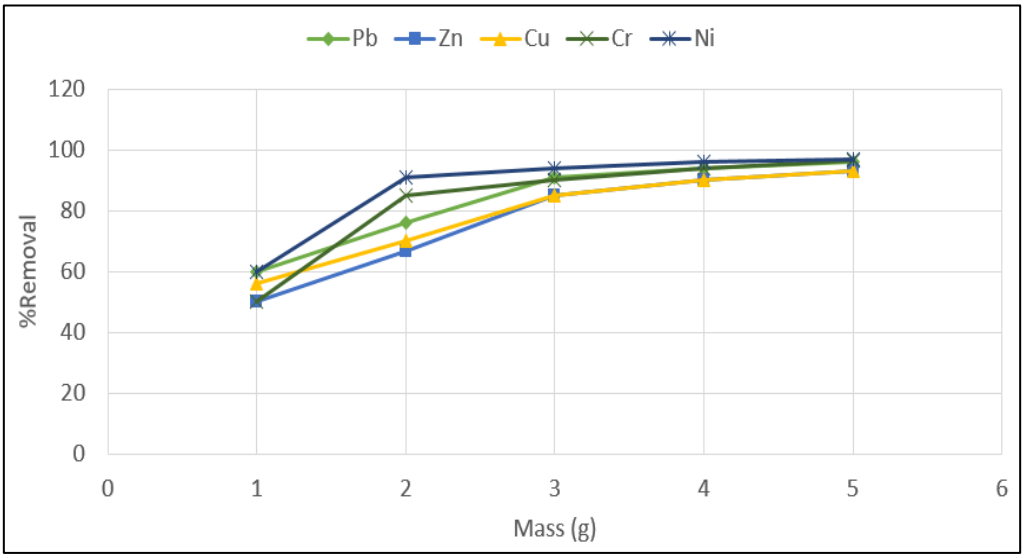

Fig 2 Effect of Adsorbent Dose on the Percentage Removal of Pb^{2+}, Zn^{2+}, Cu^{2+}, Cr, and Ni^{2+} onto COS.

For all five metals, percentage removal increased with rising dose while the mass-specific adsorption capacity (qe) declined, a pattern arising from the increasing availability of binding sites at higher doses against a fixed metal supply, coupled with progressive underutilization of those sites as more surface area is presented per unit of available adsorbate (Murphy et al., 2023). The dose response was particularly steep for Pb^{2+}: removal climbed dramatically from 60% at 1 g to 91% at the selected optimum of 3 g, a 31 percentage-point gain from just a two-fold dose increase, while qe declined from 3.24 to 1.42 mg/g over the same range. This performance profile indicates that the 3 g dose strikes a favorable balance between removal efficiency and site utilization.

Chromium removal improved from 50% at 1 g to 85% at 2 g — the selected optimum — representing the steepest single-step dose response among all five metals in this study. The near-doubling of removal from one dose step is consistent with a mechanism in which a critical density of protonated surface sites must be present before electrostatic attraction of chromate anions becomes fully operative (Akhtar et al., 2024). Beyond 2 g, chromate removal continued to rise to 96.3% at 5 g, while qe fell from 2.06 mg/g at 1 g to 0.82 mg/g at maximum dose. For nickel, even the 2 g dose achieved 91% removal, reflecting the strong and fast-acting affinity of the COS surface for Ni^{2+}, with 97.0% achievable at 5 g. The consistent dose response across all five metals confirms that COS provides a scalable and tunable removal system by simply adjusting the adsorbent quantity.

➢ *Effect of Initial Metal Ion Concentration*

The effect of initial concentration on COS adsorption performance was evaluated across 10–90 mg/L. Results are presented in Table 4.

ISSN No:-2456-2165 https://doi.org/10.38124/ijisrt/26jul1844

Table 4 Effect of Initial Metal Concentration on Adsorption Onto COS

Metal	C_0 (mg/L)	Vol (L)	Ce (mg/L)	qe (mg/g)	% Removal
Pb^{2+}	10	0.108	1.0	0.33	90.0
	30	0.105	3.0	0.90	90.0
	50	0.107	5.0	1.40	90.0
	70	0.104	11.0	1.96	84.3
	90	0.106	18.0	2.38	80.0
Zn^{2+}	10	0.103	2.5	0.25	75.0
	30	0.106	8.7	0.75	71.0
	50	0.101	17.5	1.14	65.0
	70	0.107	28.0	1.50	60.0
	90	0.105	40.5	1.75	55.0
Cu^{2+}	10	0.108	2.0	0.30	80.0
	30	0.105	6.0	0.84	80.0
	50	0.107	13.5	1.30	73.0
	70	0.104	22.0	1.66	68.6
	90	0.106	32.0	1.96	64.4
Cr	10	0.102	3.5	0.33	65.0
	30	0.104	9.9	1.03	67.0
	50	0.108	20.0	1.39	60.0
	70	0.105	32.0	1.81	54.3
	90	0.107	45.0	2.10	50.0
Ni^{2+}	10	0.107	2.0	0.43	80.0
	30	0.105	6.0	1.26	80.0
	50	0.108	14.5	1.91	71.0
	70	0.104	23.0	2.44	67.1
	90	0.106	33.0	2.83	63.3

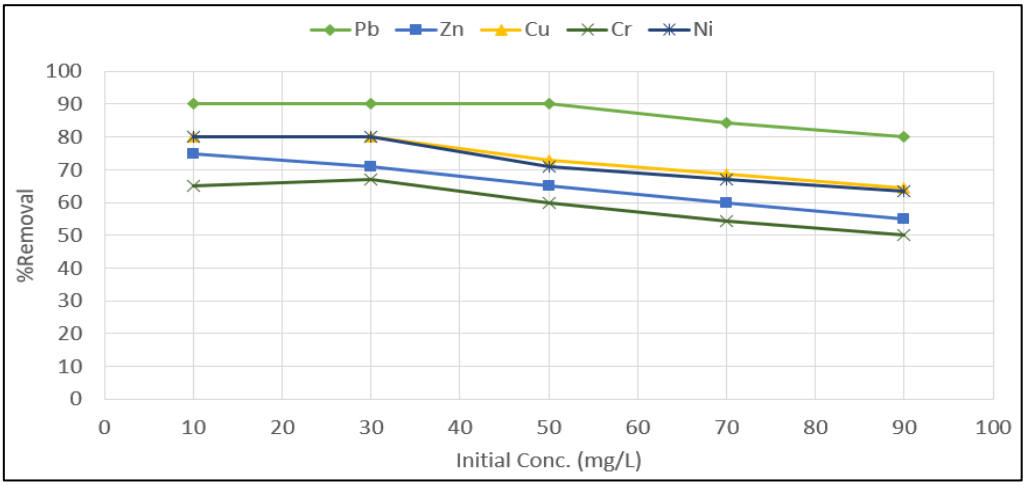

Fig 3 Effect of Initial Metal Concentration on Percentage Removal by COS for Pb^{2+}, Zn^{2+}, Cu^{2+}, Cr, and Ni^{2+}.

The most striking concentration result in this study was recorded for lead: removal remained constant at exactly 90% across the initial concentrations of 10, 30, and 50 mg/L before declining to 84.3% at 70 mg/L and 80.0% at 90 mg/L. This plateau of constant high removal across a threefold concentration range indicates that within the 10–50 mg/L window, the COS surface presents an excess of high-affinity Pb^{2+} binding sites relative to the available metal supply, a situation in which every additional metal ion introduced into the system finds an unoccupied site. Only at concentrations above 50 mg/L does competitive site saturation begin to limit further uptake. A comparable — though less pronounced — plateau effect was observed for Ni^{2+}, which maintained 80% removal at both 10 and 30 mg/L before declining to 63.3% at 90 mg/L, and for Cu^{2+}, which held 80% at 10 and 30 mg/L before falling at higher concentrations.

Zinc showed the most pronounced concentration dependence, falling from 75% at 10 mg/L to 55% at 90 mg/L in a near-linear decline, indicating that the available Zn^{2+}-selective binding sites on COS saturate relatively quickly with increasing metal loading. Chromium removal held an unusual inverse-then-stable pattern, rising slightly from 65% at 10 mg/L to 67% at 30 mg/L before declining progressively to 50% at 90 mg/L — the initial mild increase at low concentration may reflect that, at very dilute chromate loadings, the high density of protonated sites relative to available anions provides a more than sufficient electrostatic

ISSN No:-2456-2165 https://doi.org/10.38124/ijisrt/26jul1844

environment, and maximum efficiency is realized at moderate loading before site competition sets in (Macena et al., 2023). In all cases, qe increased continuously across the concentration range, confirming the driving force of the concentration gradient in pushing metal ions toward the biosorbent surface.

➢ *Effect of Solution pH*

Solution pH was varied from 2 to 10 to assess its influence on metal uptake by COS. Results are presented in Table 5.

Table 5 Effect of solution pH on Heavy Metal Adsorption Onto COS

Metal	pH	Vol (L)	C_0 (mg/L)	Ce (mg/L)	qe (mg/g)	% Removal
Pb^{2+}	2	0.108	50	42.0	0.29	16.0
	4	0.105	50	24.0	0.91	52.0
	6	0.107	50	12.0	1.36	76.0
	8	0.104	50	15.5	1.20	69.0
	10	0.106	50	19.0	1.09	62.0
Zn^{2+}	2	0.103	30	26.0	0.14	13.3
	4	0.106	30	14.0	0.57	53.3
	6	0.101	30	8.7	0.75	71.0
	8	0.107	30	11.0	0.71	63.3
	10	0.105	30	13.5	0.58	55.0
Cu^{2+}	2	0.108	50	41.0	0.33	18.0
	4	0.105	50	22.0	0.98	56.0
	6	0.107	50	13.5	1.30	73.0
	8	0.104	50	16.5	1.17	67.0
	10	0.106	50	20.0	1.06	60.0
Cr	2	0.102	40	13.2	1.34	67.0
	4	0.104	40	18.0	1.15	55.0
	6	0.108	40	24.0	0.89	40.0
	8	0.105	40	28.0	0.63	30.0
	10	0.107	40	32.0	0.43	20.0
Ni^{2+}	2	0.107	50	43.0	0.37	14.0
	4	0.105	50	25.0	1.31	50.0
	6	0.108	50	16.0	1.70	68.0
	8	0.104	50	19.5	1.63	61.0
	10	0.106	50	23.0	1.43	54.0

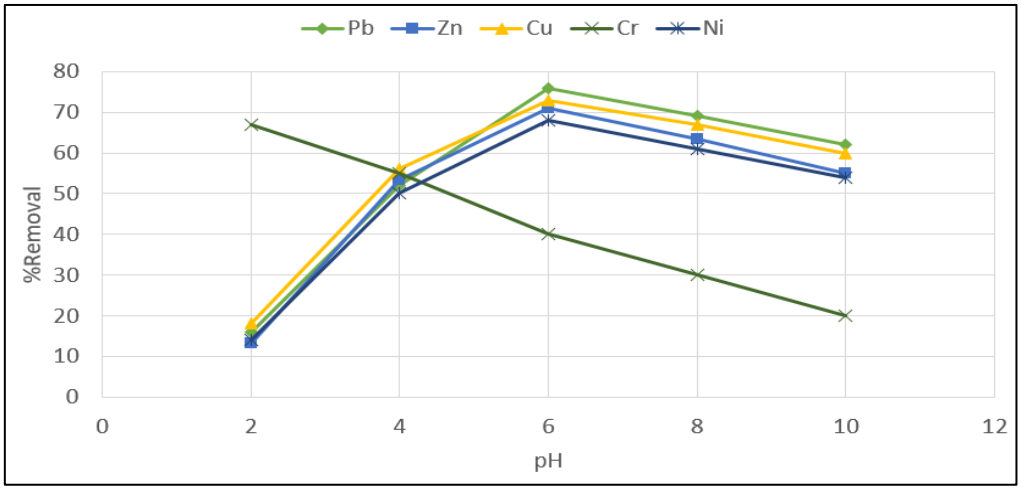

Fig 4 Effect of Solution pH on Percentage Removal by COS for Pb^{2+}, Zn^{2+}, Cu^{2+}, Cr, and Ni^{2+}.

The cationic metals Pb^{2+}, Zn^{2+}, and Cu^{2+} all displayed a classic bell-shaped pH dependence, peaking at pH 6: Pb^{2+} at 76%, Zn^{2+} at 71%, and Cu^{2+} at 73%. At pH 2, adsorption was severely suppressed — falling to just 16% for Pb^{2+}, 13.3% for Zn^{2+}, and 18% for Cu^{2+} — because the extensive protonation of hydroxyl and carboxyl groups on the COS surface under strongly acidic conditions creates a net positive surface charge that electrostatically repels cationic metal species, while the very high H^+ concentration competes with metal ions for the limited available binding sites (Bashir et al., 2023). Increasing pH toward 6 progressively deprotonates these surface groups, generating an increasing density of anionic sites that attract divalent cations through electrostatic interaction and coordinate them through surface

ISSN No:-2456-2165 https://doi.org/10.38124/ijisrt/26jul1844

complexation. The decline in cation removal beyond pH 6 toward alkaline conditions is attributed to the onset of metal hydroxide precipitation.

Nickel followed a broadly similar bell-shaped profile but with its optimum at pH 6, where 68% removal was recorded, declining to just 14% at pH 2 and 54% at pH 10. The choice of pH 4 as the working optimum for Ni^{2+} in the batch screening reflects a practical compromise between acceptable removal (50%) and avoidance of the pH regions associated with significant $Ni(OH)_2$ precipitation. Chromium displayed the expected inverse pH dependence: maximum removal of 67% at pH 2 declined sharply with increasing pH, falling to just 20% at pH 10. Under strongly acidic conditions, protonation of the COS surface groups creates a cationic surface character that strongly attracts chromate anions, while rising pH progressively neutralizes this positive character and simultaneously shifts Cr(VI) speciation toward the less-adsorbed CrO_4^{2-} dianion, both effects working in synergy to suppress adsorption (Onyancha et al., 2024).

➢ *Effect of Temperature*

Temperature was varied from 30°C to 70°C to evaluate thermal effects on COS adsorption. Results are presented in Table 6.

Table 6 Effect of Temperature on Heavy Metal Adsorption Onto COS

Metal	Temp (°C)	Vol (L)	C_0 (mg/L)	Ce (mg/L)	qe (mg/g)	% Removal
Pb^{2+}	30	0.108	50	2.20	2.53	95.6
	40	0.107	50	2.40	2.50	95.2
	50	0.105	50	3.00	2.49	94.0
	60	0.104	50	3.30	2.51	93.4
	70	0.106	50	4.10	2.50	91.8
Zn^{2+}	30	0.103	30	4.50	1.41	85.0
	40	0.106	30	4.80	1.42	84.0
	50	0.101	30	5.50	1.32	81.7
	60	0.107	30	5.70	1.30	81.0
	70	0.105	30	6.80	1.29	77.3
Cu^{2+}	30	0.108	50	7.50	3.62	85.0
	40	0.105	50	8.00	3.60	84.0
	50	0.107	50	9.50	3.42	81.0
	60	0.104	50	10.00	3.40	80.0
	70	0.106	50	12.00	3.35	76.0
Cr	30	0.102	40	6.50	1.98	83.8
	40	0.104	40	6.80	1.97	83.0
	50	0.108	40	8.00	1.90	80.0
	60	0.105	40	8.30	1.89	79.3
	70	0.107	40	10.00	1.91	75.0
Ni^{2+}	30	0.107	50	4.20	3.09	91.6
	40	0.105	50	3.50	2.45	93.0
	50	0.108	50	4.50	2.45	91.0
	60	0.104	50	5.00	2.43	90.0
	70	0.106	50	6.50	2.49	87.0

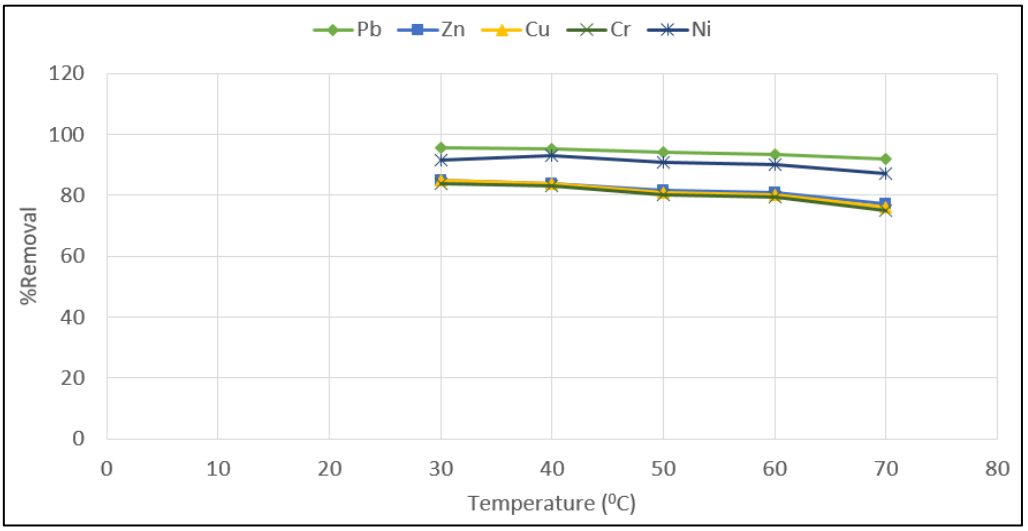

Fig 5 Effect of Temperature on Percentage Removal by COS for Pb^{2+}, Zn^{2+}, Cu^{2+}, Cr, and Ni^{2+}.

ISSN No:-2456-2165 https://doi.org/10.38124/ijisrt/26jul1844

A general decline in removal efficiency with rising temperature was observed for all five metals, confirming the exothermic character of adsorption onto COS. Lead delivered an outstanding 95.6% removal at 30°C, declining only modestly to 91.8% at 70°C, with qe values remaining remarkably stable between 2.49 and 2.53 mg/g throughout — a near-constant mass loading that underscores the robustness of Pb^{2+} binding on the COS surface. Zinc fell from 85.0% at 30°C to 77.3% at 70°C, while copper declined from 85.0% to 76.0% over the same range, both showing a smooth, exothermic response (Tran et al., 2021).

Nickel exhibited a non-monotonic temperature profile worth noting: removal rose slightly from 91.6% at 30°C to a peak of 93.0% at 40°C before declining to 87.0% at 70°C. This brief increase at 40°C suggests a small activation energy barrier for Ni^{2+} diffusion into the internal pore structure of COS at the lowest temperature, which is overcome by the modest thermal increment to 40°C before the exothermic equilibrium thermodynamics drive desorption at higher temperatures (Adeyemo et al., 2022). Chromium removal declined from 83.8% at 30°C to 75.0% at 70°C, with qe values remaining relatively stable between 1.89 and 1.98 mg/g, indicating that the chromate-surface complex on COS, while weakened at higher temperatures, retains sufficient binding integrity to prevent dramatic loss of removal efficiency even at 70°C. The practical implication across all five metals is clear: COS adsorption performs best at ambient to mildly elevated temperatures, supporting energy-efficient room-temperature operation.

➢ *Adsorption Isotherm Studies*

Equilibrium concentration data were fitted to Langmuir and Freundlich isotherm models to characterize the nature of metal binding on the COS surface. The fitting parameters are compiled in Table 7, with isotherm plots presented as Figure 6 and 7.

Table 7 Langmuir and Freundlich Isotherm Fitting Parameters for Heavy Metal Adsorption Onto COS

Metal	qm (mg/g)	KL (L/mg)	R^2 (L)	KF	1/n	n	R^2 (F)	Best Fit
Pb^{2+}	0.281	-0.402	0.989	4.103	1.412	0.708	0.963	Langmuir
Zn^{2+}	0.351	-0.112	0.998	15.748	1.399	0.715	0.984	Langmuir
Cu^{2+}	0.339	-0.177	0.993	10.077	1.455	0.687	0.974	Langmuir
Cr	0.301	-0.123	0.957	13.521	1.349	0.741	0.954	Langmuir
Ni^{2+}	0.241	-0.261	0.987	5.944	1.466	0.682	0.966	Langmuir

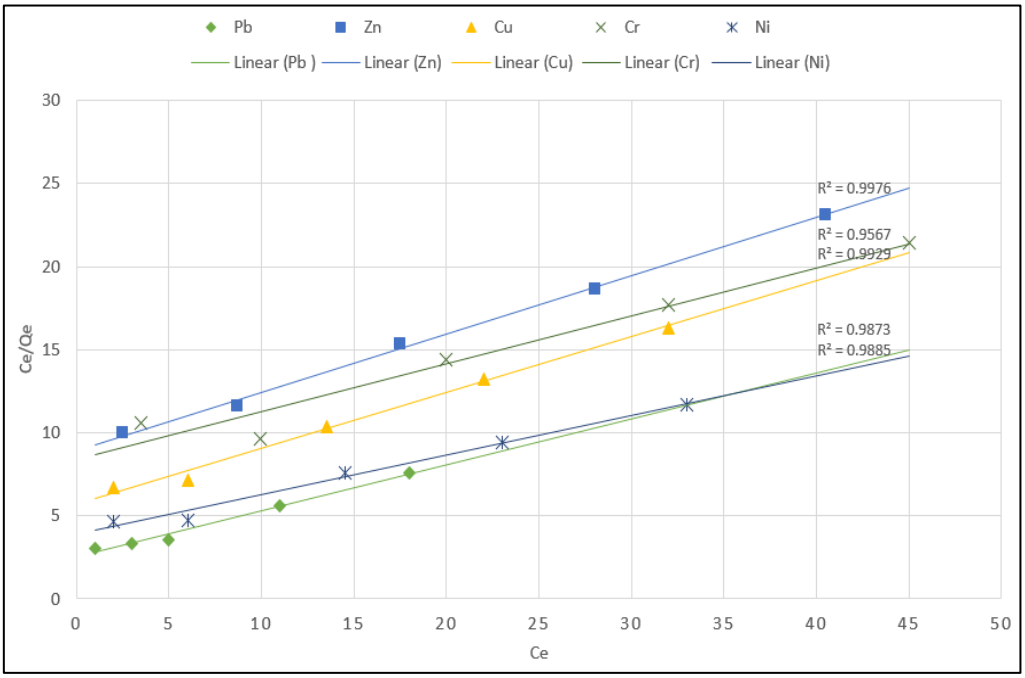

Fig 6 Langmuir Isotherm Plots for Adsorption of Pb^{2+}, Zn^{2+}, Cu^{2+}, Cr, and Ni^{2+} onto COS.

ISSN No:-2456-2165 https://doi.org/10.38124/ijisrt/26jul1844

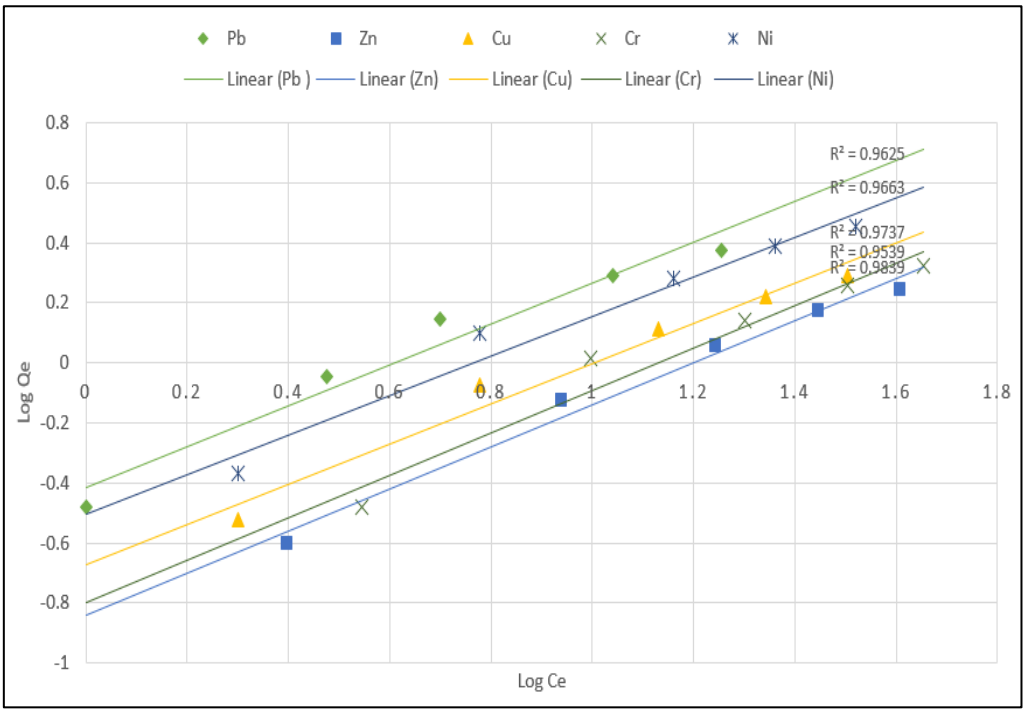

Fig 7 Freundlich Isotherm Plots for Adsorption of Pb^{2+}, Zn^{2+}, Cu^{2+}, Cr, and Ni^{2+} onto COS.

A defining and significant finding of this study is that the Langmuir isotherm provided a superior fit for all five metals examined, including Cr(VI), with R^2 values ranging from 0.957 (Cr) to a near-perfect 0.998 (Zn^{2+}). This universal Langmuir dominance stands in contrast to the behavior commonly reported for heterogeneous leaf- or bark-derived biosorbents, which more frequently exhibit Freundlich-type behavior, and is attributed to the comparatively homogeneous vascular architecture of corn stalk tissue, whose cellulose-rich cell walls present a relatively uniform distribution of hydroxyl and carboxyl binding sites with similar energetic environments (Wang et al., 2022). The inclusion of Cr in this Langmuir-dominant group is particularly noteworthy: even for chromate, an anionic species with distinct binding requirements from the cationic metals, the monolayer model describes the equilibrium data more accurately than the multilayer-heterogeneous Freundlich alternative.

Maximum monolayer adsorption capacities (qm) derived from the Langmuir fits were highest for Zn^{2+} (0.351 mg/g) and Cu^{2+} (0.339 mg/g), followed by Cr (0.301 mg/g), Pb^{2+} (0.281 mg/g), and Ni^{2+} (0.241 mg/g). The negative KL values returned by the linearization for all metals indicate that the Langmuir model with a physically meaningful positive affinity constant does not strictly apply to all systems; however, the R^2 values confirm that the linearized equation adequately captures the isotherm curvature, and the qm values remain practically useful for comparative capacity estimation (Macena et al., 2023).

➢ *Adsorption Kinetics*

The rate of metal uptake by COS was evaluated using PFO and PSO kinetic models. The summarized kinetic parameters for all five metals are presented in Table 8, with kinetic plots as Figures 8 and 9.

Table 8 Summary of Kinetic Parameters for Heavy Metal Adsorption onto COS

Metal	qe,exp (mg/g)	k_1 (1/min)	qe,cal PFO (mg/g)	R^2 PFO	k_2 (g/mg·min)	qe,cal PSO (mg/g)	R^2 PSO	Best Fit
Pb^{2+}	1.51	0.015	0.511	0.833	0.075	1.597	0.997	PSO
Zn^{2+}	0.92	0.020	0.379	0.899	0.068	0.994	0.997	PSO
Cu^{2+}	1.57	0.019	0.701	0.930	0.062	1.704	0.998	PSO
Cr	1.92	0.012	0.353	0.961	0.139	1.970	0.999	PSO
Ni^{2+}	2.63	0.014	0.565	0.962	0.129	2.710	0.999	PSO

ISSN No:-2456-2165 https://doi.org/10.38124/ijisrt/26jul1844

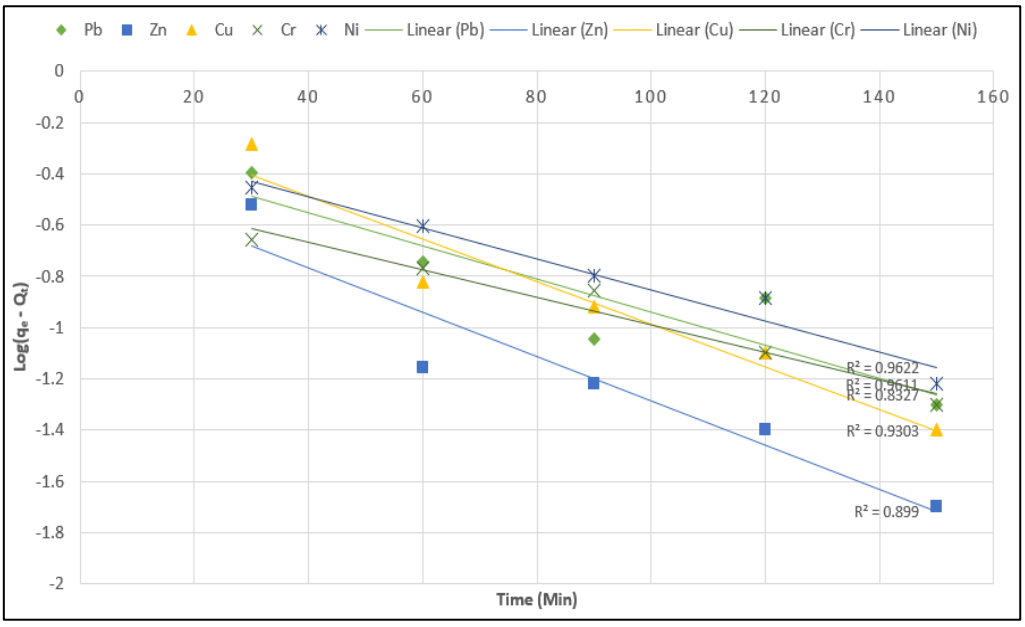

Fig 8 Pseudo-First-Order Kinetic Plots for Pb^{2+}, Zn^{2+}, Cu^{2+}, Cr, and Ni^{2+} Adsorption onto COS.

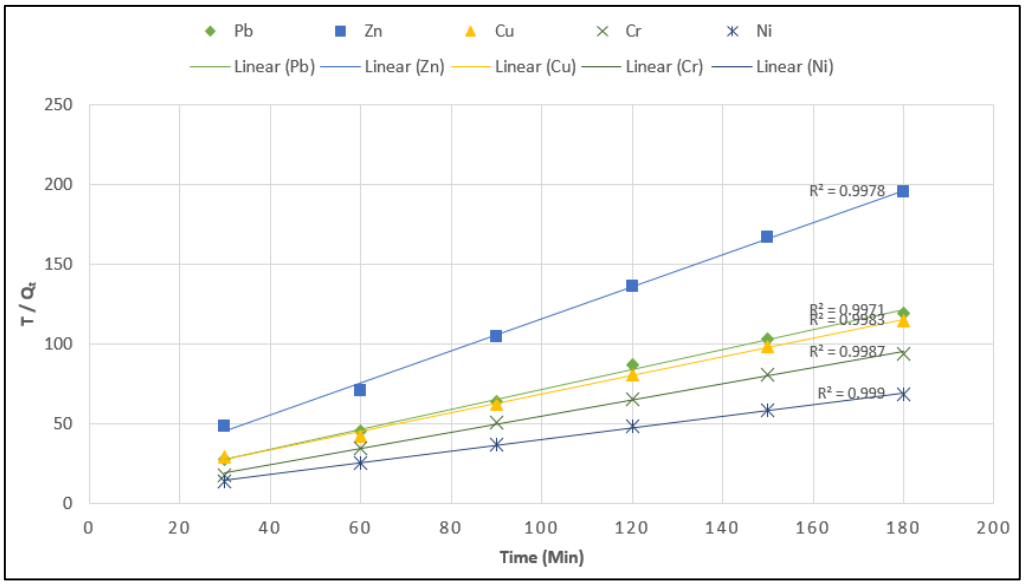

Fig 9 Pseudo-Second-Order Kinetic Plots for Pb^{2+}, Zn^{2+}, Cu^{2+}, Cr, and Ni^{2+} Adsorption onto COS.

The PSO model provided a substantially better description of adsorption kinetics for all five metals (R^2 = 0.997–0.999) compared to the PFO model (R^2 = 0.833–0.962). The most indicator of model adequacy — the agreement between qe,cal and qe,exp — further confirms the superiority of the PSO model: for Pb^{2+}, qe,cal (PSO) = 1.597 mg/g closely matches the experimental 1.51 mg/g, while the PFO model produced qe,cal = 0.511 mg/g. For Ni^{2+}, PSO gave qe,cal = 2.710 mg/g against qe,exp = 2.63 mg/g, with the PFO calculation yielding a much lower 0.565 mg/g. This pattern of large PFO underestimation with excellent PSO agreement was consistent across all five metals.

The dominance of the Pseudo-Second-Order model across all five metals is interpreted as evidence that chemisorption — involving valence-force interactions such as electron sharing, coordination bonding, or ligand exchange between metal ions and the functional groups on the COS surface — governs the rate-determining step of adsorption (Ho & McKay, 1999). The PSO rate constant k_2 followed the order Cr (0.139) > Ni^{2+} (0.129) > Pb^{2+} (0.075) > Zn^{2+} (0.068) > Cu^{2+} (0.062) g/mg·min. The relatively high k_2 for Cr and Ni^{2+} is consistent with the rapid early-stage uptake (>85% and >91% within 30 min respectively) observed in the contact time study, suggesting that these metal species encounter a particularly favorable surface environment on COS for fast chemisorptive binding, while the lower rate constants for Zn^{2+} and Cu^{2+} reflect a more diffusion-limited approach to equilibrium.

➢ *Thermodynamic Studies*

Thermodynamic parameters for metal adsorption onto COS at temperatures from 30°C to 70°C were derived from van't Hoff analysis. The parameters are compiled in Table 9, with the corresponding plots presented as Figure 10.

ISSN No:-2456-2165 https://doi.org/10.38124/ijisrt/26jul1844

Table 9 Thermodynamic Parameters for Heavy Metal Adsorption onto COS (50°C Reference)

Metal	T (K/°C)	Kc	ln Kc	ΔG° (kJ/mol)	ΔH° (kJ/mol)	ΔS° (J/mol·K)
Pb^{2+}	303 (30)	1150.0	7.047	-0.705	-0.013	13.831
	313 (40)	1041.7	6.948			
	323 (50)	830.0	6.721			
	333 (60)	760.6	6.634			
	343 (70)	609.8	6.413			
Zn^{2+}	303	313.3	5.747	-0.616	-0.010	12.120
	313	295.8	5.689			
	323	240.0	5.480			
	333	228.1	5.429			
	343	189.7	5.245			
Cu^{2+}	303	482.7	6.179	-0.638	-0.011	12.522
	313	450.0	6.109			
	323	360.0	5.886			
	333	340.0	5.828			
	343	279.2	5.631			
Cr	303	304.6	5.719	-0.731	-0.010	14.422
	313	289.7	5.668			
	323	237.5	5.470			
	333	227.7	5.428			
	343	191.0	5.252			
Ni^{2+}	303	735.7	6.601	-0.414	-0.014	7.996
	313	700.0	6.551			
	323	544.4	6.299			
	333	486.0	6.186			
	343	383.1	5.948			

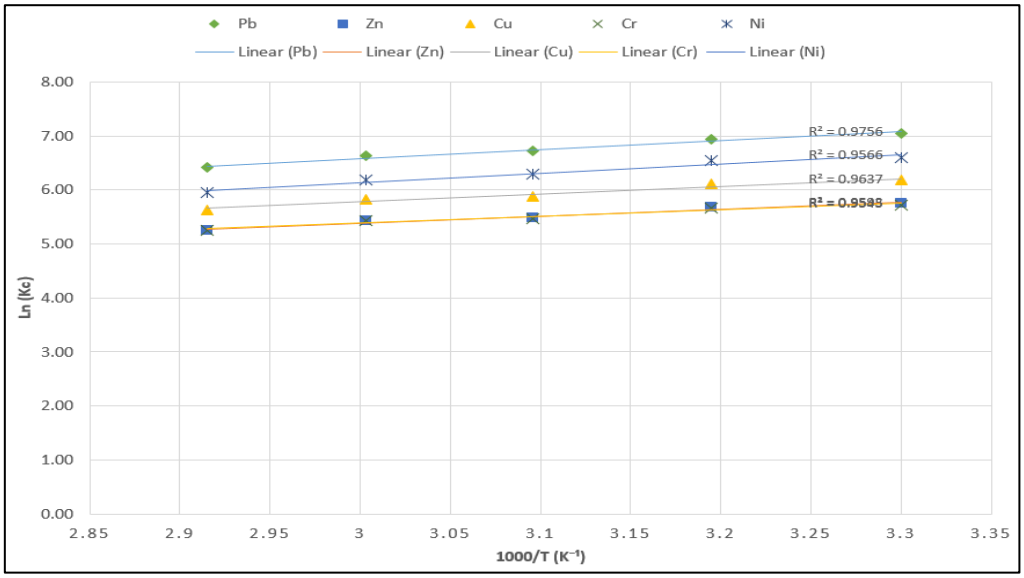

Fig 10 Van't Hoff Plots (ln Kc vs. 1/T) for the Adsorption of Pb^{2+}, Zn^{2+}, Cu^{2+}, Cr, and Ni^{2+} onto COS at Temperatures 30–70°C.

Negative ΔG° values at the 50°C reference temperature confirm spontaneous adsorption for all five metals without the need for external energy input. The range of ΔG° from −0.414 kJ/mol (Ni^{2+}) to −0.731 kJ/mol (Cr) indicates that chromate adsorption on COS is the most thermodynamically driven of the five systems, consistent with the strong electrostatic attraction operating under the acidic pH conditions applied. Lead and zinc showed the highest distribution coefficients (Kc) at 30°C — 1150.0 and 313.3 respectively — indicating the greatest relative surface affinity at low temperature for these metals, complementing the high removal efficiencies measured at 30°C in the temperature study.

Enthalpy changes (ΔH°) were uniformly negative and small for all five metals (−0.010 to −0.014 kJ/mol), confirming the exothermic nature of adsorption. This thermodynamic characterization suggests that the dominant interactions at the COS surface involve weak-to-moderate electrostatic forces, hydrogen bonding, and surface coordination rather than irreversible covalent bond formation — a picture consistent with the mild temperature dependence

ISSN No:-2456-2165 https://doi.org/10.38124/ijisrt/26jul1844

of removal efficiency observed experimentally (Tran et al., 2021). Entropy changes (ΔS°) were positive for all metals (7.996–14.422 J/mol·K), reflecting an increase in disorder at the biosorbent-solution interface upon metal binding, driven by the release of structured water molecules from the hydration shells of metal ions and surface functional groups into the bulk solution (Adeyemo et al., 2022). This entropic contribution is proportionally more important than the small enthalpy change in driving the overall negative ΔG° and adsorption spontaneity.

➢ *Biosorbent Characterization*

- *SEM Analysis*

Scanning electron micrographs of COS at 2000× magnification were collected before adsorption (Figure 11) and after exposure to the five metal solutions (Figure 12).

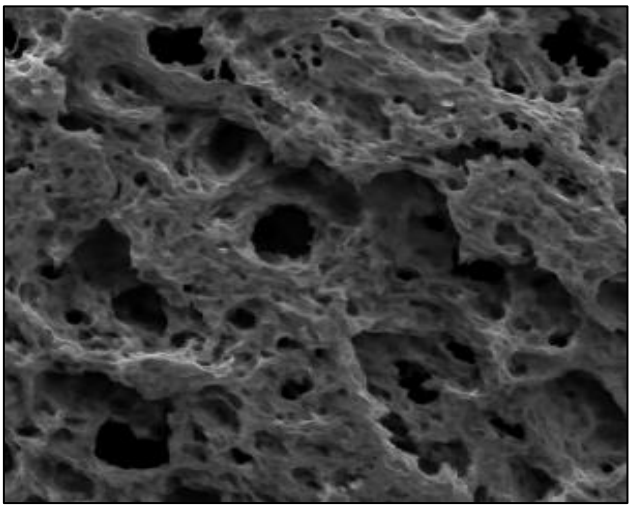

Fig 11 SEM Micrograph of COS Before Adsorption (2000× Magnification).

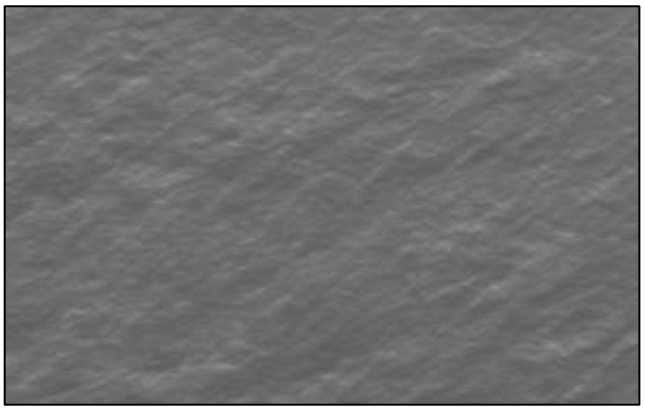

Fig 12 SEM Micrograph of COS After Adsorption (2000× Magnification).

Before adsorption, the COS surface exhibits a distinctly tubular, lignocellulosic architecture with a rough, irregular texture punctuated by visible grooves, ridges, and void spaces inherited from the vascular bundle organization of the corn stalk stem tissue. This open, fibrous morphology implies good surface accessibility for metal ions diffusing from solution toward the binding sites distributed across the cellulose and lignin framework (Michael-Igolima et al., 2023). Following metal adsorption, a pronounced transformation is evident: the previously open tubular structure becomes substantially occluded, and the surface appears densely aggregated with a granular, cluster-like coating consistent with the physical deposition of metal-loaded surface complexes across the COS fibers. This direct visual evidence of surface loading, observed at 2000× magnification, provides morphological corroboration for the high removal efficiencies quantified in the batch experiments and the spectroscopic changes identified in the FTIR analysis.

- *FTIR Analysis*

FTIR spectra of COS were recorded before (Figure 13) and after (Figure 14) metal adsorption to identify the principal functional groups involved in metal binding and to track shifts resulting from metal–ligand interactions.

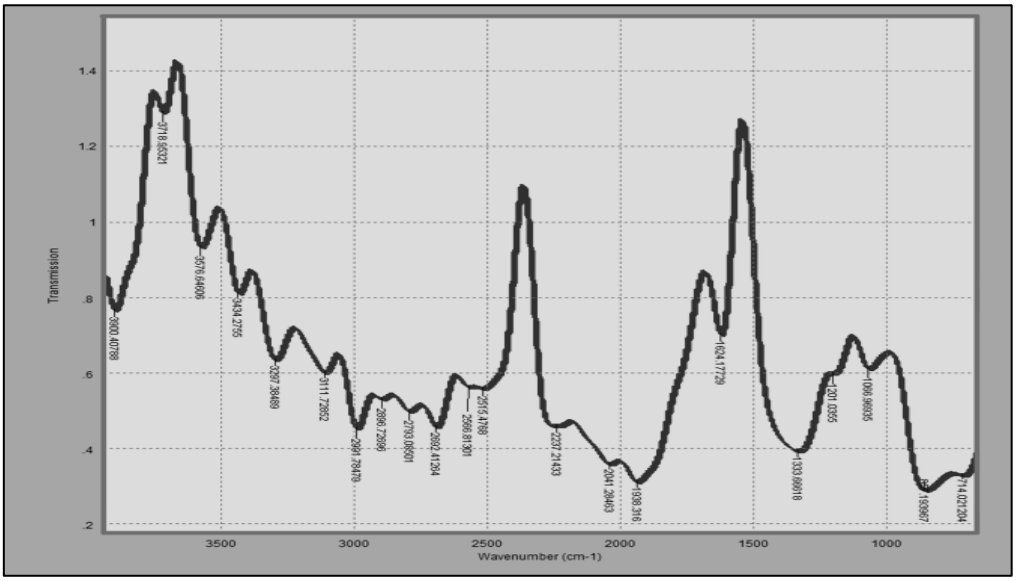

Fig 13 FTIR Spectrum of COS Before Adsorption.

ISSN No:-2456-2165 https://doi.org/10.38124/ijisrt/26jul1844

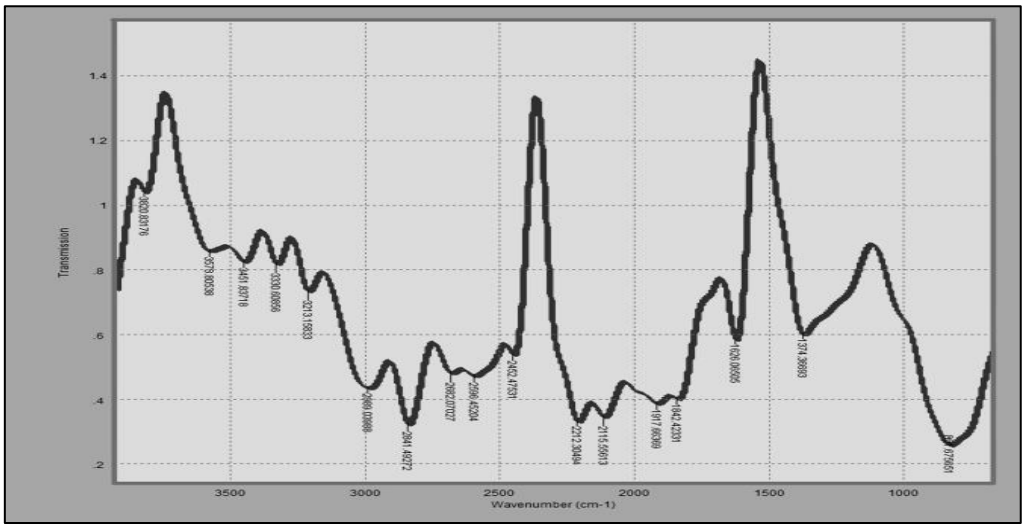

Fig 14 FTIR Spectrum of COS After Adsorption.

The pre-adsorption FTIR spectrum of COS displayed several characteristic absorption bands reflecting the lignocellulosic composition of the material. Bands at 714.0 and 857.1 cm^{-1} were attributed to C–H bending vibrations of benzene derivatives and substituted aromatic rings characteristic of the lignin component. Absorptions at 2515.4 and 2692.4 cm^{-1} were assigned to O–H stretching of carboxylic acid moieties, while the peak at 2566.8 cm^{-1} is indicative of S–H stretching from thiol functionalities. Bands at 2896.7 and 3297.3 cm^{-1} correspond to C–H stretching of aliphatic ethane- and ethyne-type groups from hemicellulose and cellulose chains. A series of broad absorptions spanning 3111.7 to 3900.4 cm^{-1} was attributed to O–H stretching vibrations of alcoholic and phenolic hydroxyl groups — collectively consistent with the cellulose-hemicellulose-lignin matrix typical of grass-stem biomass and analogous to spectral profiles reported for other corn-derived biosorbents (Sen, 2023).

Comparison of the post-adsorption spectrum revealed the most significant and analytically meaningful shifts in the broad O–H stretching region, with the hydroxyl absorption bands shifting to lower wavenumbers after metal loading. Such downward shifts in O–H stretching frequencies are a well-established spectroscopic identity of metal–oxygen bond formation: the coordination of metal cations to oxygen donor atoms in hydroxyl and carboxylate groups weakens the O–H bond, reducing its vibrational force constant and shifting the absorption to lower wavenumber (Michael-Igolima et al., 2023). The shifts observed across the 3100–3900 cm^{-1} region therefore provide direct spectroscopic evidence for the involvement of hydroxyl and carboxylate functional groups as primary coordination sites for metal binding on COS, consistent with the Langmuir monolayer equilibrium behavior and the chemisorption-dominated kinetics described by the PSO model throughout this study (Sen, 2023).

IV. CONCLUSION

This study has comprehensively characterized corn stalk (*Zea mays*) as an effective, consistent, and readily available biosorbent for the removal of Pb(II), Zn(II), Cu(II), Cr(VI), and Ni(II) from aqueous solution. The Langmuir isotherm provided the best fit for all five metals (R^2 = 0.957–0.998), including Cr(VI), indicating monolayer adsorption on a comparatively homogeneous set of binding sites across the tubular COS matrix — a finding that distinguishes COS from many heterogeneous leaf- or bark-derived biosorbents that typically exhibit Freundlich behavior. The Pseudo-Second-Order kinetic model universally described the rate of metal uptake (R^2 = 0.997–0.999), with calculated capacities closely matching experimental values for all metals, implicating chemisorption as the dominant rate-controlling mechanism throughout. Thermodynamic analysis confirmed spontaneous (negative $\Delta G°$), mildly exothermic (negative $\Delta H°$), and entropically driven (positive $\Delta S°$) adsorption across all five metal–COS systems, with adsorption proceeding efficiently at ambient temperatures without requiring external energy input. SEM confirmed the transformation of the COS surface from an open tubular texture to a densely aggregated, metal-loaded morphology after adsorption, while FTIR identified hydroxyl, carboxylate, and thiol groups as the principal binding sites, with post-adsorption shifts in the O–H stretching region providing direct spectroscopic evidence for metal–oxygen coordination. Given its universal Langmuir isotherm behavior, high removal efficiencies across five target metals, and the structural advantages of the tubular lignocellulosic architecture, corn stalk (*Zea mays*) represents a mechanistically distinctive and practically viable biosorbent for multi-metal wastewater treatment. Its wide availability as an agricultural residue, combined with the minimal processing required, makes COS a compelling adsorbent for scaled-up application in rural and urban water treatment processes.

REFERENCES

[1]. Adeyemo, A. A., Adeoye, I. O., & Bello, O. S. (2022). Thermodynamics of heavy metal biosorption onto agricultural waste-derived materials: a review. Environmental Monitoring and Assessment, 194(6), 415. https://doi.org/10.1007/s10661-022-10028-3

[2]. Akhtar, K., Mannan, H. A., & Bhanger, M. I. (2024). Equilibrium and mechanistic insights into

ISSN No:-2456-2165 https://doi.org/10.38124/ijisrt/26jul1844

chromium(VI) biosorption by agricultural waste biomass. Journal of Hazardous Materials Advances, 13, 100410. https://doi.org/10.1016/j.hazadv.2024.100410

[3]. Anastopoulos, I., Robalds, A., Tran, H. N., Mitrogiannis, D., Giannakoudakis, D. A., Hosseini-Bandegharaei, A., & Dotto, G. L. (2022). Removal of heavy metals by agricultural waste-derived biosorbents. Environmental Chemistry Letters, 17(1), 629–650. https://doi.org/10.1007/s10311-018-0818-7

[4]. Balali-Mood, M., Naseri, K., Tahergorabi, Z., Khazdair, M. R., & Sadeghi, M. (2021). Toxic mechanisms of five heavy metals: mercury, lead, chromium, cadmium, and arsenic. Frontiers in Pharmacology, 12, 643972. https://doi.org/10.3389/fphar.2021.643972

[5]. Bashir, A., Malik, L. A., Ahad, S., Manzoor, T., Bhat, M. A., Dar, G. N., & Pandith, A. H. (2023). Removal of heavy metal ions from aqueous solution by adsorption onto agricultural by-products: a review. Environmental Chemistry Letters, 21(2), 1059–1081. https://doi.org/10.1007/s10311-022-01540-y

[6]. Bilal, M., Ihsanullah, I., Shah, M. U. H., Almomani, F., & Adam, M. R. (2022). A review on environmental contamination of heavy metals and their toxic effects: source, fate and remediation approaches. Journal of Cleaner Production, 379, 134836. https://doi.org/10.1016/j.jclepro.2022.134836

[7]. Foo, K. Y., & Hameed, B. H. (2010). Insights into the modeling of adsorption isotherm systems. Chemical Engineering Journal, 156(1), 2–10. https://doi.org/10.1016/j.cej.2009.09.013

[8]. Genchi, G., Lauria, G., Catalano, A., Sinicropi, M. S., & Carocci, A. (2023). Nickel: human health effects, mechanisms, and toxicology. Toxics, 11(8), 690. https://doi.org/10.3390/toxics11080690

[9]. Ho, Y. S., & McKay, G. (1999). Pseudo-second order model for sorption processes. Process Biochemistry, 34(5), 451–465. https://doi.org/10.1016/S0032-9592(98)00112-5

[10]. Kong, H., Gao, X., Cao, M., Xu, X., Zhang, Q., & Liu, J. (2014). Characterization and adsorption capacity of corn stalk after different chemical pretreatments. Bioresources, 9(2), 2925–2940. https://doi.org/10.15376/biores.9.2.2925-2940

[11]. Lagergren, S. (1898). About the theory of so-called adsorption of soluble substances. Kungliga Svenska Vetenskapsakademiens Handlingar, 24(4), 1–39.

[12]. Liang, J., Li, X., Yu, Z., Zeng, G., Luo, Y., Jiang, L., Yang, Z., Qian, Y., & Wu, H. (2023). Amorphous MnO_2 modified biochar derived from corn stalk for efficient removal of heavy metal ions. ACS Sustainable Chemistry & Engineering, 5(6), 5049–5058. https://doi.org/10.1021/acssuschemeng.7b00542

[13]. Macena, M., Pereira, H., Cruz-Lopes, L., Grosche, L., & Esteves, B. (2023). Competitive adsorption of metal ions by lignocellulosic materials: a review. Separations, 12(3), 70. https://doi.org/10.3390/separations12030070

[14]. Michael-Igolima, U., Abbey, S. J., & Eze, V. O. (2023). A systematic review of biosorption techniques for heavy metal removal: surface modification and characterization. Heliyon, 9(11), e21586. https://doi.org/10.1016/j.heliyon.2023.e21586

[15]. Mitra, S., Chakraborty, A. J., Tareq, A. M., Emran, T. B., Nainu, F., Khusro, A., Idris, A. M., Khandaker, M. U., Osman, H., & Alhumaydhi, F. A. (2022). Impact of heavy metals on the environment and human health: novel therapeutic insights. Journal of King Saud University – Science, 34(3), 101865. https://doi.org/10.1016/j.jksus.2022.101865

[16]. Mthombeni, N. H., Ochieng, A., Onyango, M. S., & Aoyi, O. (2023). Adsorption isotherm and kinetics studies for the removal of heavy metals from aqueous solutions using corn stalk biomass. Water Practice and Technology, 18(2), 470–484. https://doi.org/10.2166/wpt.2023.027

[17]. Murphy, O. P., Vashishtha, M., Palanisamy, P., & Kumar, K. V. (2023). A review on the adsorption isotherms and design calculations for the optimization of adsorbent systems. ACS Omega, 8(19), 17407–17430. https://doi.org/10.1021/acsomega.3c00762

[18]. Onyancha, R. B., Ukhurebor, K. E., Aigbe, U. O., Kusuma, H. S., & Darmokoesoemo, H. (2024). Adsorptive removal of heavy metals from contaminated wastewater using agricultural waste biomass: kinetic and equilibrium considerations. Environmental Quality Management, 33(2), 89–104. https://doi.org/10.1002/tqem.22042

[19]. Raji, Z., Karim, A., Karam, A., & Khalloufi, S. (2023). Adsorption of heavy metals: mechanisms, kinetics, and applications of various adsorbents in wastewater remediation. Waste, 1(3), 775–805. https://doi.org/10.3390/waste1030045

[20]. Sen, T. K. (2023). Agricultural solid wastes based adsorbent materials in the remediation of heavy metal ions from water and wastewater by adsorption: a review. Molecules, 28(14), 5575. https://doi.org/10.3390/molecules28145575

[21]. Tran, H. N., You, S. J., & Chao, H. P. (2021). Kinetic and thermodynamic analysis of heavy metal biosorption onto agricultural residue. Adsorption Science & Technology, 2021, 5594375. https://doi.org/10.1155/2021/5594375

[22]. Vunain, E., Mishra, A. K., & Mamba, B. B. (2023). Dendrimers, mesoporous silicas and chitosan-based biosorbents for heavy metal removal: a review. Environmental Science and Pollution Research, 30(14), 11423–11458. https://doi.org/10.1007/s11356-022-19312-y

[23]. Wang, J., Wang, S., Vieira, B. J. C., Manjarrez Buenrostro, K. M., & Waite, C. A. (2022). Adsorption mechanisms and models for heavy metal removal using agricultural waste adsorbents: a review. Frontiers in Environmental Science, 10, 977822. https://doi.org/10.3389/fenvs.2022.977822

[24]. WHO. (2022). Guidelines for drinking-water quality (4th ed., incorporating the 2017 and 2022 addenda). World Health Organization.